

# Inferring the magnetic anisotropy of a nanosample through dynamic cantilever magnetometry measurements

Cite as: Appl. Phys. Lett. **116**, 193102 (2020); doi: [10.1063/5.0004598](https://doi.org/10.1063/5.0004598)

Submitted: 13 February 2020 · Accepted: 6 May 2020 ·

Published Online: 14 May 2020





View Online



Export Citation



CrossMark

Yang Yu,<sup>1,2,3</sup> Feng Xu,<sup>1,2,3</sup> Shanshan Guo,<sup>4,5,6</sup> Ning Wang,<sup>1,3</sup> Lvquan Zou,<sup>1,3,a)</sup>  Baomin Wang,<sup>4,5</sup>  Run-Wei Li,<sup>4,5</sup> and Fei Xue<sup>1,3,b)</sup> 

## AFFILIATIONS

<sup>1</sup>Anhui Province Key Laboratory of Condensed Matter Physics at Extreme Conditions, High Magnetic Field Laboratory, Chinese Academy of Sciences, Hefei 230031, People's Republic of China

<sup>2</sup>University of Science and Technology of China, Hefei 230026, People's Republic of China

<sup>3</sup>Collaborative Innovation Center of Advanced Microstructures, Nanjing University, Nanjing 210093, People's Republic of China

<sup>4</sup>CAS Key Laboratory of Magnetic Materials and Devices, Ningbo Institute of Materials Technology and Engineering, Chinese Academy of Sciences, Ningbo 315201, People's Republic of China

<sup>5</sup>Zhejiang Province Key Laboratory of Magnetic Materials and Application Technology, Ningbo Institute of Materials Technology and Engineering, Chinese Academy of Sciences, Ningbo 315201, People's Republic of China

<sup>6</sup>University of Chinese Academy of Sciences, Beijing 100049, People's Republic of China

<sup>a)</sup>zoulvquan@hmfl.ac.cn

<sup>b)</sup>Author to whom correspondence should be addressed: xuef@hmfl.ac.cn

## ABSTRACT

The magnetic anisotropy of bit-patterned media, such as a mesocrystal, is a key parameter in spintronics. Here, we utilize the high sensitivity of dynamic cantilever magnetometry to investigate the foundation of a mesocrystal, an individual  $\text{CoFe}_2\text{O}_4$  pyramid nanocrystal. The magnetic anisotropy of the nanosample can be inferred through quantitatively correlating the main features in the evolution of the magnetic energy with frequency shifts in dynamic cantilever magnetometry measurements. Magnetometry data taken at 280 K exhibit hybrid magnetic anisotropy, including uniaxial anisotropy and cubic anisotropy. Low-temperature measurements further confirm the previously reported single-domain state and indicate that the cubic anisotropy is mainly magnetocrystalline anisotropy, while uniaxial anisotropy is likely to be induced by the interface between the  $\text{CoFe}_2\text{O}_4$  pyramid and the  $\text{BiFeO}_3$  layer. The analysis provides an alternative interpretation for dynamic cantilever magnetometry data, which may extend the application of magnetometry.

Published under license by AIP Publishing. <https://doi.org/10.1063/5.0004598>

Magnetic anisotropy, including magnetocrystalline anisotropy, shape anisotropy, magnetoelastic anisotropy, exchange bias, and induced magnetic anisotropy, is a key feature of magnetic materials. It gives rise to the magnetism of permanent magnets and also plays an important role in recently popular spintronics, as represented by the giant magnetoresistance effect.<sup>1,2</sup> Motivated by industrial interest in magnetic storage and sensors,<sup>3–6</sup> research into magnetic anisotropy in low-dimensional materials, especially in thin films, has been flourishing in recent decades.

Several breakthroughs have improved the stability and recording density of magnetic materials, e.g., exchange bias<sup>7,8</sup> and perpendicular magnetic anisotropy,<sup>9,10</sup> which is manifested in the

form of spin-valve-based devices including magnetic random access memory and spin-transfer torque magnetic random access memory.<sup>11</sup> The performance can be enhanced using an elegant design of the recording media structure, such as bit-patterned media (BPM),<sup>12–15</sup> in which one single bit of information is stored in an individual nanostructure.<sup>16,17</sup> However, conventional fabricated BPM contain isolated polycrystal islands, so that the switching field has a wide distribution due to the nonuniform microstructure.

Recently, a unique crystallographically hierarchical structure that was made of isolated well-organized nanocrystals, called mesocrystals, was synthesized by a one-step self-assembly crystallization process.<sup>18</sup>

We further developed the method and fabricated 2D magnetic  $\text{CoFe}_2\text{O}_4$  (CFO) mesocrystals, which protrude from the substrate surface with perfect crystal facets, specific crystallographic orientation, and fully relaxed stress.<sup>19</sup> To test the quality of BPM or magnetic sensors made of a single nanocrystal, it is essential to know the magnetic anisotropy of an individual nanomagnet. This cannot be roughly extrapolated from conventional measurements of ensembles like a vibrating-sample magnetometer or a superconducting quantum interference device (SQUID) because of sample-to-sample inhomogeneities in size, shape, orientation, and dipole interaction between the nanomagnets. In this work, we investigate the magnetic anisotropy of such an individual nanocrystal using dynamic cantilever magnetometry (DCM) because of its high sensitivity.<sup>20</sup>

In previous studies, two approaches for analyzing DCM measurements created an analytical model based on the Stoner–Wohlfarth approximation or numerical simulations.<sup>21–26</sup> The samples are mainly nanowires or nanotubes, which naturally exhibit uniaxial anisotropy. In fact, it is not easy for samples with other forms of anisotropy to exhibit an explicit frequency shift.<sup>27</sup> In our earlier work,<sup>28</sup> there was some evidence for biaxial anisotropy in a rectangular Co thin film.

The CFO mesocrystals were fabricated through a combination of the growth of a nanoseed layer and the self-assembly of oxides.<sup>19</sup> An individual CFO nanomagnet was prepared and transferred onto an ultrasoft cantilever for the DCM experiments using a FEI Helios NanoLab 600i focused ion beam and a scanning electron microscope (SEM) dual-beam system.<sup>38</sup> The single-crystal silicon cantilever used here was  $147\ \mu\text{m}$  long,  $4\ \mu\text{m}$  wide, and  $0.1\ \mu\text{m}$  thick. The cantilever used in our experiments has a resonant frequency of  $f_0 = 2612\ \text{Hz}$  and a spring constant of  $k_0 = 43\ \mu\text{N/m}$ . The frequency of the cantilever was measured using a home-built microlens fiber-optic interferometer system. The interferometer has a  $1550\ \text{nm}$  laser with an incident laser power of less than  $1\ \mu\text{W}$ . The DCM experiments were carried out in a vacuum chamber with the pressure below  $1 \times 10^{-6}$  mbar. A superconducting vector magnet produced a magnetic field of up to  $9\ \text{T}$  along the vertical  $z$ -axis and  $1\ \text{T}$  along the horizontal  $x$ - and  $y$ -axes. The orientation of the CFO nanopyramid on the cantilever is shown in Fig. 1(a). The single-domain CFO nanopyramid has an edge length of  $87\ \text{nm}$ .<sup>19</sup> One edge of the bottom plane was attached to the cantilever, and the height of the nanopyramid was parallel to the length of the cantilever. In the main text, we discuss only data for  $H$  applied along the vertical  $z$ -axis. Measurement data for  $H$  in the other directions are discussed in the [supplementary material](#).

Figure 2 shows the measured frequency shift at  $280\ \text{K}$ . Unlike previously reported data where  $\Delta f$  monotonically increases with the magnetic field strength,<sup>22,28</sup> the frequency shift seems to be relatively insensitive to the magnetic field except for four sharp peaks, which are labeled T1, T2, T3, and T4 in ascending order of field strength for convenience. The observed data indicate that an explicit hybrid anisotropy term, rather than a sum or integral of several influences, contributes to the frequency of the single-crystal CFO nanopyramid. Here, we speculate on the nature of this hybrid anisotropy, which can be verified by comparing the four measured peaks and additional data (see the [supplementary material](#)) with the predictions of the model. We can calculate the anisotropy parameters using this hybrid anisotropy and experimental data.

Although solving the frequency shift as a function of the magnetic field is rather challenging,<sup>27</sup> the peaks can still be regarded as

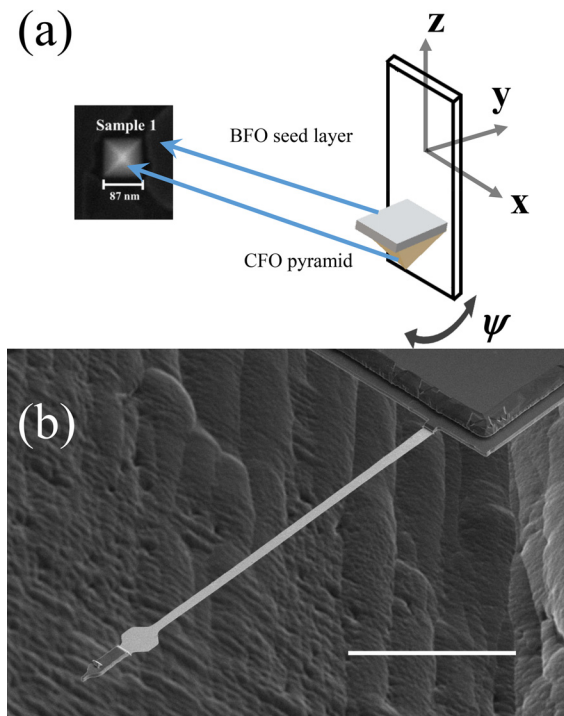


**FIG. 1.** (a) Schematic of dynamic cantilever magnetometry (DCM). The inset shows a scanning electron microscope (SEM) image of an individual  $\text{CoFe}_2\text{O}_4$  pyramid nanocrystal with a  $\text{BiFeO}_3$  seed layer. (b) SEM image of the pyramid on a cantilever. Scale bar:  $50\ \mu\text{m}$ .

solid evidence of magnetization jumps. As a reasonable approximation, we neglect the oscillations of the cantilever and consider only static magnetization as the cause of the magnetization jumps.

For simplicity, a spherical coordinate system is established [Fig. 3(a)]. The speculated energy of the system can be written as the sum of the cantilever energy, the Zeeman energy, and the magnetic anisotropy energy,

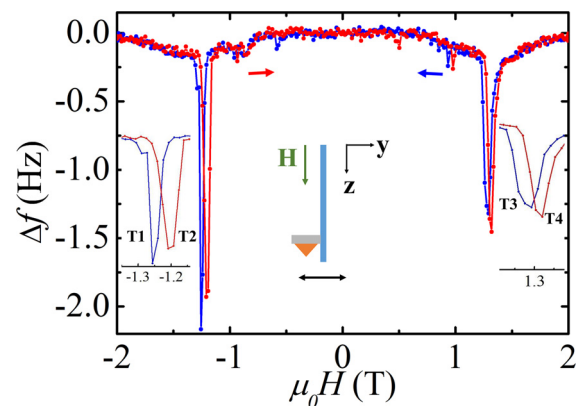


**FIG. 2.** Experimental frequency shift  $\Delta f$  as a function of magnetic field  $H$ . The red (blue) curve is for  $H$  sweeps in the positive (negative) direction. The enlarged insets represent detailed  $\Delta f$  vs  $H$  at transition points with magnetization jumps.

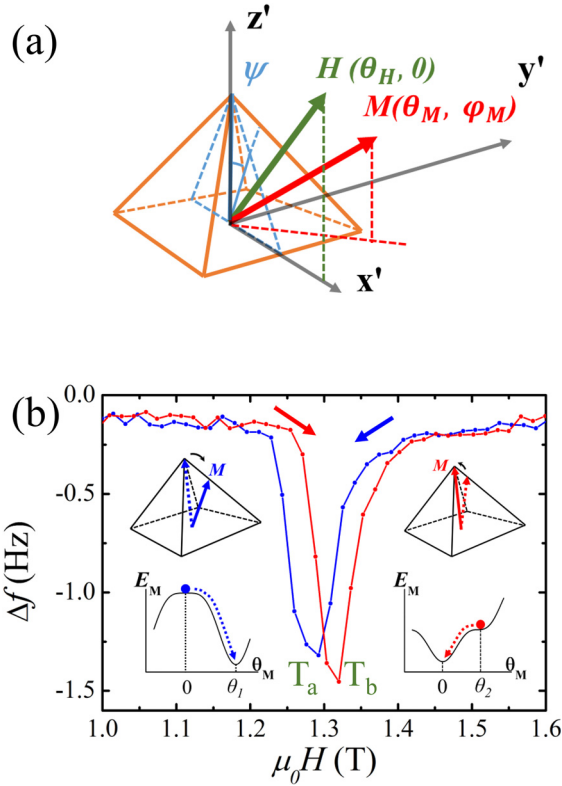


**FIG. 3.** Theoretical interpretation of the frequency peak as a magnetization jump. (a) Spherical coordinate system for the oscillating sample. The orange pyramid is the CFO nanomagnet. The red and green arrows are the magnetization and magnetic field, respectively. The blue triangle is the oscillating plane of the cantilever, and  $\psi$  is the oscillating angle. (b) Magnetic energy profile and jump derived from the hybrid anisotropy model at transition points  $T_a$  and  $T_b$ . The points and curves are experimental data as a reference.

$$\begin{aligned}
 E = & \frac{1}{2}k_0(l_e\psi)^2 - MVH(\sin\psi\sin\theta_M\cos\varphi_M + \cos\psi\cos\theta_M) \\
 & + K_{\text{cubic}}V\left(\frac{1}{4}\sin^4\theta_M\cos^22\varphi_M + \sin^2\theta_M\cos^2\theta_M\right) \\
 & - K_{\text{in}}V\sin^2\theta_M, \quad (1)
 \end{aligned}$$

where  $k_0$  is the intrinsic spring constant of the cantilever,  $l_e$  is the effective length of the cantilever, and  $V$  is the volume of the pyramid. The third term describes the cubic magnetic anisotropy energy, including magnetocrystalline anisotropy and shape anisotropy. As half of an octahedron, the nanomagnet is believed to have a cubic shape anisotropy based on the method of images.<sup>29</sup> Since  $\text{CoFe}_2\text{O}_4$  has cubic magnetocrystalline anisotropy,<sup>30</sup> the total magnetic anisotropy energy is cubic and the coefficient  $K_{\text{cubic}}$  is the sum of the shape anisotropy constant  $K_{\text{shape}}$  and the magnetocrystalline anisotropy constant  $K_{\text{cryst}}$ . The fourth term gives the uniaxial anisotropy.<sup>31</sup>

Here, we describe the theoretical magnetic behavior predicted by this hybrid anisotropy to analyze how magnetization jumps occur. For simplicity, we discuss the frequency peak for the positive magnetic field ( $H > 0$ ), as the magnetic behavior is symmetric with respect to the magnetic field.

Conventionally, the equilibrium state of magnetization can be obtained by setting the first derivative of energy with respect to the magnetization angle to zero. In fact,  $\varphi_M = 45^\circ$  is always a solution for  $\partial E/\partial\varphi_M = 0$ . Moreover, the detailed analysis of the local minimum of energy in the [supplementary material](#) indicates that the motion of the magnetization is inplane.

Figure 3(b) shows the theoretical energy profile near the transition points. The experimental data are also plotted as a reference. When the magnetic field decreases to a critical value  $T_a$ , the magnetization state becomes an inflection point and can jump from  $\theta_M = 0$  to  $\theta_M = \theta_1$ . The magnetic free-energy profile at  $T_a$  is illustrated in the bottom left inset. On increasing the magnetic field,  $M$  will experience a different jump from  $\theta_M = \theta_2$  to  $\theta_M = 0$  at transition point  $T_b$ . Like other magnetic phenomena, the magnetic free-energy profile depends on the magnetization history. Thus, the  $T_a$ -type profile occurs for decreasing  $|H|$ , whereas the  $T_b$ -type profile occurs for increasing  $|H|$ . Note that the four magnetization jumps occur only when the ratio of the two anisotropy constants  $K_{\text{in}}/K_{\text{cubic}}$  falls into a certain range. Besides, the absolute value of the critical magnetic field at  $T_b$  is always larger than that at  $T_a$ . The [supplementary material](#) includes a video showing the evolution of the magnetic energy as the magnetic field increases. The magnetization jump is a direct result of competition between the Zeeman energy and the hybrid anisotropy energy.

Now, we consider the experimental data shown in Fig. 2. According to the field sweeping direction, T2 and T3 are  $T_a$ -type transitions, while T1 and T4 are  $T_b$ -type transitions. Consistent with the theory, the observed absolute value of the critical magnetic field at T1 or T4 is indeed larger than that at T2 or T3 (see Fig. S4). This evidence, along with further supporting data in the [supplementary material](#), forms a solid demonstration of the validity of the anisotropy model.

Since the measured frequency shift is confirmed by the model, it is possible to calculate the anisotropy constant from the critical magnetic field strength. Starting from the reduced magnetic energy,

$$\begin{aligned}
 E_M = & \frac{(E - (1/2)k_0(l_e\psi)^2)}{K_{\text{cubic}}V} \\
 = & -n(\sin\psi\sin\theta_M\cos\varphi_M + \cos\psi\cos\theta_M) \\
 & + \frac{1}{4}\sin^4\theta_M\cos^22\varphi_M \\
 & + \sin^2\theta_M\cos^2\theta_M - m\sin^2\theta_M, \quad (2)
 \end{aligned}$$

where  $n(H) = MH/K_{\text{cubic}}$  and  $m = K_{\text{in}}/K_{\text{cubic}}$ . Here, we consider static cantilever magnetometry, and so  $\psi = 0^\circ$ . Since the magnetization has an inplane motion, as discussed before,  $\varphi_M = 45^\circ$  is a constant.  $E_M$  can be simplified as

$$E_M = -n\cos\theta_M + \sin^2\theta_M\cos^2\theta_M - m\sin^2\theta_M. \quad (3)$$

We first analyze the experimental data for a positive magnetic field [Fig. 3(b)]. Both transition points  $T_a$  and  $T_b$  are inflection points. They satisfy

$$\frac{\partial E_M}{\partial\theta_M} = (n + \cos\theta_M - 2m\cos\theta_M + \cos3\theta_M)\sin\theta_M = 0, \quad (4a)$$

$$\frac{\partial^2 E_M}{\partial\theta_M^2} = n\cos\theta_M - 2m\cos2\theta_M + 2\cos4\theta_M = 0. \quad (4b)$$

There are two sets of solutions for Eq. (4). One is

$$\theta_M = 0^\circ, \quad (5a)$$

$$n = 2m - 2. \quad (5b)$$

This is exactly the expression for transition point  $T_a$ . The other solution, which corresponds to  $T_b$ , is a little more complicated,

$$\theta_M = \arctan \sqrt{\frac{5-m}{1+m}}, \quad (6a)$$

$$n = \frac{1}{9} \left( 3\sqrt{6}\sqrt{1+m} + 3\sqrt{6}m\sqrt{1+m} - \sqrt{6}(1+m)^{3/2} \right). \quad (6b)$$

We can find  $m$  using the ratio of the two critical magnetic field strengths ( $H_{T_a} = 1.285$  T and  $H_{T_b} = 1.312$  T),

$$\frac{2m-2}{(1/9) \left( 3\sqrt{6}\sqrt{1+m} + 3\sqrt{6}m\sqrt{1+m} - \sqrt{6}(1+m)^{3/2} \right)} = \frac{1.285}{1.312}. \quad (7)$$

Thus,  $m$  can be found numerically,

$$m = 3.83. \quad (8)$$

Also, the two angles  $\theta_1$  and  $\theta_2$  can be calculated. Using  $n = 5.66$  and  $m = 3.83$  in Eq. (4a),  $\theta_1$  can be calculated to be  $37.8^\circ$ . According to Eq. (6),  $\theta_2 = 26.2^\circ$ .

The anisotropy constants can be calculated using

$$K_{\text{cubic}} = \frac{1}{n|_{H_{T_a}}} MH_{T_a} = \frac{1}{n|_{H_{T_b}}} MH_{T_b}, \quad (9a)$$

$$K_{\text{in}} = mK_{\text{cubic}}. \quad (9b)$$

Here,  $n|_{H_{T_a}}$  and  $n|_{H_{T_b}}$  are the values of  $n$  when  $H$  is  $H_{T_a}$  and  $H_{T_b}$ , respectively. Considering saturated magnetization in Eq. (9),<sup>19</sup> we have  $K_{\text{cubic}} = 2.3 \times 10^6$  erg/cm<sup>3</sup> and  $K_{\text{in}} = 8.8 \times 10^6$  erg/cm<sup>3</sup>. The corresponding anisotropy fields are  $H_{\text{cubic}} = 2K_{\text{cubic}}/M = 4.6$  kOe and  $H_{\text{in}} = 2K_{\text{in}}/M = 17.6$  kOe.

The experimental data for a negative magnetic field can be explained by applying this method with  $\theta_M = 180^\circ$ . Similar conclusions can be made.

To investigate the physical origin of anisotropy, we measured the frequency shift at low temperatures. The variation of  $m = K_{\text{in}}/K_{\text{cubic}}$  with respect to temperature  $T$  can be obtained, as shown in Fig. 4(a). The temperature dependence of the cubic anisotropy field is plotted in Fig. 4(b). As the temperature decreases,  $H_{\text{cubic}}$  gradually increases until 260 K and shows a drastic elevation to a maximum value at 230 K. As the temperature further decreases,  $H_{\text{cubic}}$  drops moderately. Since shape anisotropy is induced by surface magnetic free poles,  $K_{\text{shape}}$  is proportional to the square of  $M$ . Thus, the  $H_{\text{shape}}$  vs  $T$  curve just reflects the dependence of the magnetization on temperature. As reported in the literature,<sup>32</sup> the magnetization increases monotonically as the temperature decreases. Thus, the cubic magnetic anisotropy is dominated by magnetocrystalline anisotropy  $K_{\text{cryst}}$ . In fact, similar behavior has been observed in cobalt-doped magnetite due to the Verwey transition.<sup>30,33</sup>

The uniaxial magnetic anisotropy field  $H_{\text{in}}$ , which is  $m$  times the cubic anisotropy field, has a more complex dependence on

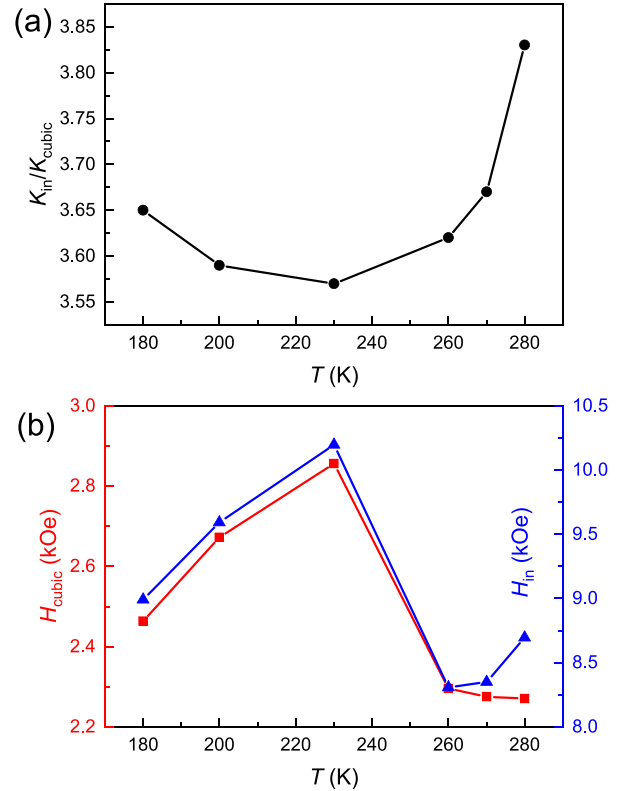


**FIG. 4.** Temperature dependence from 180 to 280 K of (a)  $m = K_{\text{in}}/K_{\text{cubic}}$  and (b) the cubic anisotropy field  $H_{\text{cubic}}$  (red squares) and uniaxial anisotropy field  $H_{\text{in}}$  (blue triangles). The non-monotonic behavior of the cubic anisotropy field can be attributed to the Verwey transition of the  $\text{CoFe}_2\text{O}_4$  crystal.

temperature [Fig. 4(b)]. A possible physical origin of the uniaxial anisotropy is an interfacial effect arising from the coupling between the  $\text{CoFe}_2\text{O}_4$  pyramid and the  $\text{BiFeO}_3$  seed layer. The coupling may also account for the slight exchange bias in the measured frequency shift (Fig. S4). In fact, extensive research has unveiled several phenomena associated with the interface between  $\text{BiFeO}_3$  and ferromagnetic materials, by mechanisms like exchange bias and superexchange coupling due to the charge transfer or electronic orbital reconstruction at the interface.<sup>34–36</sup>

As the temperature decreases further, the frequency shifts at 4 K and 10 K (see the [supplementary material](#)) do not exhibit four sharp peaks compared to those at high temperatures, but resemble the result for the sample with uniaxial anisotropy. This is consistent with the analysis for  $H_{\text{cubic}}$  vs  $T$  at high temperatures. Below the Verwey point, the crystal transforms into a structure with a lower symmetry, so that the magnetocrystalline anisotropy becomes uniaxial.<sup>37</sup>

The robustness and generalization of our model were further demonstrated by measurements made with the magnetic field applied in the other two orientations, which is comprehensively discussed in the [supplementary material](#). We also performed an experiment with another CFO sample, the data for which have already been published.<sup>19,38</sup> The calculated  $m = K_{\text{in}}/K_{\text{cubic}} = 4$  is comparable with  $m = 3.8$  here.



In conclusion, we have presented a method for investigating the magnetic anisotropy of nanosamples based on DCM. By quantitatively correlating the main features observed in the evolution of the trial magnetic anisotropy energy using DCM measurements, the magnetic anisotropy constants can be calculated for critical magnetic field strengths. In this work, we applied this method to an individual  $\text{CoFe}_2\text{O}_4$  (CFO) nanopillar sample. The magnetic anisotropy was demonstrated to be hybrid, with a cubic term and a uniaxial term. The temperature dependence of the anisotropy suggests that the cubic term  $K_{\text{cubic}}$  is dominated by magnetocrystalline anisotropy, whereas the uniaxial term  $K_{\text{in}}$  may be induced by coupling between the CFO pillar and the  $\text{BiFeO}_3$  seed layer at the interface. Our work provides an insightful perspective for contemporary DCM research.

See the [supplementary material](#) for more information on the samples and the setup, more DCM data and discussions for H in other directions, and DCM data and discussions for low temperatures.

The authors thank Professor M. Poggio for providing the ultrasoft cantilevers used in these experiments. This work was supported by the National Key Research and Development Program of China (Grant Nos. 2017YFA0303201 and 2016YFA0201102) and the National Natural Science Foundation of China (Grant Nos. 11374305, 11604338, 51871232, and 11704386). A portion of this work was supported by the High Magnetic Field Laboratory of Anhui Province.

#### DATA AVAILABILITY

The data that support the findings of this study are available from the corresponding author upon reasonable request.

#### REFERENCES

- 1M. N. Baibich, J. M. Broto, A. Fert, F. Nguyen Van Dau, F. Petroff, P. Eitenne, G. Creuzet, A. Friederich, and J. Chazelas, *Phys. Rev. Lett.* **61**, 2472 (1988).
- 2G. Binash, P. Grünberg, F. Saurenbach, and W. Zinn, *Phys. Rev. B* **39**, 4828 (1989).
- 3C. Chappert, A. Fert, and F. Nguyen Van Dau, *Nat. Mater.* **6**, 813 (2007).
- 4A. Manchon, H. C. Koo, J. Nitta, S. M. Frolov, and R. A. Duine, *Nat. Mater.* **14**, 871 (2015).
- 5T. Jungwirth, J. Wunderlich, and K. Olejník, *Nat. Mater.* **11**, 382 (2012).
- 6T. Jungwirth, J. Wunderlich, V. Novák, K. Olejník, B. L. Gallagher, R. P. Campion, K. W. Edmonds, A. W. Rushforth, A. J. Ferguson, and P. Némec, *Rev. Mod. Phys.* **86**, 855 (2014).
- 7W. H. Meiklejohn and C. P. Bean, *Phys. Rev.* **105**, 904 (1957).
- 8Y. Shiratsuchi, H. Noutomi, H. Oikawa, T. Nakamura, M. Suzuki, T. Fujita, K. Arakawa, Y. Takechi, H. Mori, T. Kinoshita, M. Yamamoto, and R. Nakatani, *Phys. Rev. Lett.* **109**, 077202 (2012).
- 9S. Ikeda, K. Miura, H. Yamamoto, K. Mizunuma, H. D. Gan, M. Endo, S. Kanai, J. Hayakawa, F. Matsukura, and H. Ohno, *Nat. Mater.* **9**, 721 (2010).
- 10B. Dieny and M. Chshiev, *Rev. Mod. Phys.* **89**, 025008 (2017).
- 11S. Bhatti, R. Sbiaa, A. Hirohata, H. Ohno, S. Fukami, and S. N. Piramanayagam, *Mater. Today* **20**, 530 (2017).
- 12T. R. Albrecht, H. Arora, V. Ayanoor-Vitikate, J.-M. Beaujour, D. Bedau, D. Berman, A. L. Bogdanov, Y.-A. Chapuis, J. Cushen, E. E. Dobisz, G. Doerk, H. Gao, M. Grobis, B. Gurney, W. Hanson, O. Hellwig, T. Hirano, P.-O. Jubert, D. Kercher, J. Lille, Z. Liu, C. M. Mate, Y. Obukhov, K. C. Patel, K. Rubin, R. Ruiz, M. Schabes, L. Wan, D. Weller, T.-W. Wu, and E. Yang, *IEEE Trans. Magn.* **51**, 0800342 (2015).
- 13A. Kikitsu, *J. Magn. Magn. Mater.* **321**, 526 (2009).
- 14D. Weller, H. Brändle, G. Gorman, C.-J. Lin, and H. Notarys, *Appl. Phys. Lett.* **61**, 2726 (1992).
- 15H. J. Richter, *J. Magn. Magn. Mater.* **321**, 467 (2009).
- 16R. L. White, R. M. H. New, and R. F. W. Pease, *IEEE Trans. Magn.* **33**, 990 (1997).
- 17H. J. Richter, A. Y. Dobin, O. Heinonen, K. Z. Gao, and R. J. M. vd Veerdonk, *IEEE Trans. Magn.* **42**, 2255 (2006).
- 18H. Cölfen and M. Antonietti, *Angew. Chem., Int. Ed.* **44**, 5576 (2005).
- 19S. S. Guo, F. Xu, B. M. Wang, N. Wang, H. L. Yang, P. Dhanapal, F. Xue, J. L. Wang, and R. W. Li, *Adv. Mater. Interfaces* **5**, 1800997 (2018).
- 20B. C. Stipe, H. J. Mamin, T. D. Stowe, T. W. Kenny, and D. Rugar, *Phys. Rev. Lett.* **86**, 2874 (2001).
- 21A. Buchter, J. Nagel, D. Ruffer, F. Xue, D. P. Weber, O. F. Kieler, T. Weimann, J. Kohlmann, A. B. Zorin, E. Russo-Averchi, R. Huber, P. Berberich, A. Fontcuberta i Morral, M. Kemmler, R. Kleiner, D. Koelle, D. Grundler, and M. Poggio, *Phys. Rev. Lett.* **111**, 067202 (2013).
- 22D. P. Weber, D. Ruffer, A. Buchter, F. Xue, E. Russo-Averchi, R. Huber, P. Berberich, J. Arbiol, A. Fontcuberta i Morral, D. Grundler, and M. Poggio, *Nano Lett.* **12**, 6139 (2012).
- 23B. Gross, D. P. Weber, D. Ruffer, A. Buchter, F. Heimbach, A. Fontcuberta i Morral, D. Grundler, and M. Poggio, *Phys. Rev. B* **93**, 064409 (2016).
- 24A. Mehlin, F. Xue, D. Liang, H. F. Du, M. J. Stolt, S. Jin, M. L. Tian, and M. Poggio, *Nano Lett.* **15**, 4839 (2015).
- 25N. Shamsudhin, Y. Tao, J. Sort, B. Jang, C. L. Degen, B. J. Nelson, and S. Pané, *Small* **12**, 6363 (2016).
- 26A. Mehlin, B. Gross, M. Wyss, T. Schefer, G. Tütüncüoğlu, F. Heimbach, A. Fontcuberta i Morral, D. Grundler, and M. Poggio, *Phys. Rev. B* **97**, 134422 (2018).
- 27A. Kamra, M. Schreier, H. Huebl, and S. T. B. Goennenwein, *Phys. Rev. B* **89**, 184406 (2014).
- 28Y. Yu, F. Xu, N. Wang, L. K. Zou, and F. Xue, *Jpn. J. Appl. Phys., Part 1* **57**, 090312 (2018).
- 29B. D. Cullity and C. D. Graham, *Introduction to Magnetic Materials* (John Wiley & Sons, 2005).
- 30J. C. Slonczewski, *J. Appl. Phys.* **32**, S253 (1961).
- 31M. Tejedro, J. A. García, J. Carrizo, L. Elbaile, J. D. Santos, J. Mira, and J. Rivas, *J. Appl. Phys.* **86**, 2185 (1999).
- 32H. Shenker, *Phys. Rev.* **107**, 1246 (1957).
- 33K. Abe, Y. Miyamoto, and S. Chikazumi, *J. Phys. Soc. Jpn.* **41**, 1894 (1976).
- 34T. Gao, X. Zhang, W. Ratcliff, S. Maruyama, M. Murakami, A. Varatharajan, Z. Yamani, P. Chen, K. Wang, H. Zhang, R. Shull, L. A. Bendersky, J. Unguris, R. Ramesh, and I. Takeuchi, *Nano Lett.* **17**, 2825 (2017).
- 35F. A. Cuellar, Y. H. Liu, J. Salafranca, N. Nemes, E. Iborra, G. Sanchez-Santolino, M. Varela, M. G. Hernandez, J. W. Freeland, M. Zhernenkov, M. R. Fitzsimmons, S. Okamoto, S. J. Pennycook, M. Bibes, A. Barthélémy, S. G. E. Te Velthuis, Z. Sefrioui, C. Leon, and J. Santamaria, *Nat. Commun.* **5**, 4215 (2014).
- 36F. Y. Bruno, M. N. Grisolia, C. Visani, S. Valencia, M. Varela, R. Abrudan, J. Tornos, A. Rivera-Calzada, A. A. Únal, S. J. Pennycook, Z. Sefrioui, C. Leon, J. E. Villegas, J. Santamaria, A. Barthélémy, and M. Bibes, *Nat. Commun.* **6**, 6306 (2015).
- 37E. J. W. Verwey and P. W. Haayman, *Physica* **8**, 979 (1941).
- 38F. Xu, S. S. Guo, Y. Yu, N. Wang, L. K. Zou, B. M. Wang, R. W. Li, and F. Xue, *Phys. Rev. Appl.* **11**, 054007 (2019).